JCTC Journal of Chemical Theory and Computation

ARTICLE

pubs.acs.org/JCTC

Diabatization Schemes for Generating Charge-Localized Electron−Proton Vibronic States in Proton-Coupled Electron Transfer Systems

Andrew Sirjoosingh and Sharon Hammes-Schiffer*

Department of Chemistry, 104 Chemistry Building, Pennsylvania State University, University Park, Pennsylvania 16802, United States

Supporting Information

ABSTRACT: A scheme for the rigorous construction of charge-localized diabatic electron−proton vibronic states for proton-coupled electron transfer (PCET) reactions is presented. The diabatic electronic states are calculated using an adiabatic-to-diabatic transformation designed to ensure that the first-order nonadiabatic couplings with respect to a specified one-dimensional reaction coordinate vanish exactly. This scheme is applied to both symmetric and asymmetric PCET systems with several different one-dimensional reaction coordinates, including the hydrogen transfer coordinate, a normal mode coordinate, and the intrinsic reaction coordinate. This approach is also extended to describe the three-dimensional motion of the transferring hydrogen. The diabatic electronic states exhibit relatively invariant charge distributions along the reaction coordinate and are in excellent agreement with the analogous states obtained from the generalized Mulliken−Hush and Boys localization methods. Furthermore, these diabatic electronic states are combined with the associated proton vibrational wave functions to generate charge-localized electron−proton vibronic states that describe one- or three-dimensional hydrogen motion. These electron−proton vibronic states can be used to calculate the vibronic couplings, rate constants, and kinetic isotope effects of PCET reactions.

I. INTRODUCTION

Proton-coupled electron transfer (PCET) reactions are prevalent in many facets of biology, chemistry, and physics.[1−5] Concerted PCET reactions, which are characterized by simultaneous electron and proton transfer without a stable intermediate, have been observed in a wide variety of systems, including enzymatic, photoinduced, and electrochemical processes. Typically, PCET reactions are characterized as vibronically nonadiabatic because the subsystem comprised of the electrons and transferring proton does not respond instantaneously to the motions of the solvent and other solute nuclei. Within this nonadiabatic framework, PCET theories require the identification of the charge-localized reactant and product diabatic electron−proton vibronic states corresponding to the transferring electron and proton localized on their donors and acceptors, respectively.[2,6] These diabatic electron−proton vibronic states can be used to calculate the vibronic couplings, which are key quantities in the nonadiabatic PCET rate constant expressions derived with the golden rule formalism.[7,8] Combined with the solute and solvent reorganization energies, as well as the vibronic energy level splittings, these vibronic couplings can be used to calculate experimentally accessible quantities such as rate constants and kinetic isotope effects.

The objective of this paper is to develop a methodology for the rigorous construction of the charge-localized diabatic electron−proton vibronic states that form the basis of nonadiabatic PCET theories. A variety of schemes have been developed to generate diabatic electronic states, particularly for electron transfer reactions.[9−31] Diabatic electronic states can be defined mathematically as states with vanishing first-order nonadiabatic couplings at all possible nuclear configurations. In the context of electron transfer reactions, the diabatic electronic states are associated with the physically meaningful reactant and product states corresponding to the electron localized on the donor and acceptor, respectively. These diabatic electronic states are usually characterized by charge invariance in that the electronic charge distribution does not change significantly with nuclear motion. Schemes that have been developed to generate charge-localized diabatic electronic states for electron transfer reactions include the minimization of first-order nonadiabatic couplings using an adiabatic electronic state basis,[10−12] the generalized Mulliken−Hush method[13,14] and extensions using Boys localization,[25,26] block diagonalization methods,[19,20] approaches enforcing configurational uniformity,[9,16,17,22] constrained density functional theory,[29,30] and valence bond theory approaches.[15,24]

In a previous study,[23] we devised a scheme to calculate charge-localized diabatic electronic states for PCET reactions. In particular, we used an adiabatic-to-diabatic transformation[10] to generate diabatic electronic states constructed to ensure that the first-order nonadiabatic couplings with respect to the one-dimensional transferring hydrogen coordinate vanish exactly. When this diabatization approach was applied to the phenoxyl−phenol self-exchange PCET reaction, the diabatic electronic states were shown to exhibit physically meaningful charge-localized electronic charge distributions. Moreover, we showed that this diabatization scheme provides quantitative diagnostics for the degree of electron−proton nonadiabaticity in PCET systems.[23] Identifying the degree of electron−proton nonadiabaticity is important because this property impacts the form of

Received: May 27, 2011
Published: July 28, 2011

ACS Publications © 2011 American Chemical Society

the vibronic coupling and the rate constant and provides insight into the fundamental mechanism. Specifically, electronically adiabatic proton transfer is associated with the hydrogen atom transfer mechanism, which does not involve significant electronic charge redistribution, and electronically nonadiabatic proton transfer is associated with the PCET mechanism, which involves significant electronic charge redistribution.[32,33]

In the present study, we expand this diabatization scheme in several directions. We extend this approach to general asymmetric PCET reactions and to other one-dimensional reaction coordinates, such as a normal mode coordinate or the intrinsic reaction coordinate (IRC). We also expand the previous treatment to describe three-dimensional hydrogen motion, where the component of the first-order nonadiabatic coupling vector along a specified one-dimensional reaction coordinate vanishes rigorously for all points on the three-dimensional diabatic electronic surfaces. In addition, we devise a strategy that utilizes the diabatic electronic states, along with the associated proton vibrational wave functions, to construct electron−proton vibronic states that describe either one-dimensional or three-dimensional hydrogen motion. These electron−proton vibronic states form the basis of nonadiabatic PCET theories and enable the calculation of vibronic couplings, rate constants, and kinetic isotope effects.

In addition to developing these extensions of the diabatization method for PCET reactions, we compare the diabatic electronic states obtained with this approach to those obtained with the generalized Mulliken−Hush (GMH) method[13,14] and extensions using Boys localization.[25,26] These alternative diabatization methods generate the diabatic electronic states from the dipole moments associated with the ground and excited adiabatic electronic states rather than the first-order nonadiabatic couplings. The application of the GMH and Boys localization diabatization methods to PCET reactions is straightforward but, to our knowledge, has not been explored previously. The similarities among the diabatic electronic states generated with these three different diabatization methods provide a degree of validation for the underlying assumptions of the theoretical treatments.

An outline of this paper is as follows. Section II.A describes the adiabatic-to-diabatic transformation along a one-dimensional hydrogen coordinate utilized to generate diabatic electronic states. In section II.B, we discuss modifications of this diabatization protocol to generate diabatic electronic states along general one-dimensional reaction coordinates, including a normal mode coordinate and the IRC. Section II.C describes the construction of diabatic electron−proton vibronic states for both one-dimensional and three-dimensional hydrogen motion. Section II.D summarizes the GMH and Boys localization methods that are implemented for comparison. In section III, we provide the details of the computational methods used to study three model PCET systems: the phenoxyl−phenol self-exchange reaction, the asymmetric phenoxyl−quinol reaction, and the amidinium−carboxylate system representing an experimentally studied photoinduced PCET reaction.[34−36] Section IV.A describes the generation of the diabatic electronic states for these three model systems, illustrating the extensions to asymmetric systems and to alternative one-dimensional reaction coordinates. Section IV.B presents the strategy for combining the diabatic electronic states with the associated proton vibrational states to construct diabatic electron−proton vibronic states. In section IV.C, we provide a comparison of this diabatization method to the GMH and Boys localization methods for generating diabatic electronic states. Finally, conclusions and future direction are discussed in section V.

II. THEORY

II.A. Adiabatic-to-Diabatic Transformation. Consider a system comprised of N_e electrons, N_p protons, and N_s slow nuclei with coordinates $\mathbf{r}_e$, $\mathbf{r}_p$, and $\mathbf{R}$ and masses m_e, m_p, and $\{M_I\}$, respectively, and with potential energy $V(\mathbf{r}_e,\mathbf{r}_p,\mathbf{R})$. The Hamiltonian for the "fast" degrees of freedom (i.e., the electron−proton subsystem) is

$$H_q = -\sum_{i'=1}^{N_p} \frac{\hbar^2}{2m_p}\nabla_{i'}^2 + H_e \tag{1}$$

where the electronic Hamiltonian is

$$H_e = -\sum_{i=1}^{N_e} \frac{\hbar^2}{2m_e}\nabla_i^2 + V(\mathbf{r}_e,\mathbf{r}_p,\mathbf{R}) \tag{2}$$

For fixed $\mathbf{R}$, the eigenfunctions $\{\Phi_k(\mathbf{r}_e;\mathbf{r}_p;\mathbf{R})\}$ of H_q are calculated by solving

$$H_q\Phi_k(\mathbf{r}_e,\mathbf{r}_p;\mathbf{R}) = E_k(\mathbf{R})\ \Phi_k(\mathbf{r}_e,\mathbf{r}_p;\mathbf{R}) \tag{3}$$

The adiabatic electronic states for fixed $(\mathbf{r}_p,\mathbf{R})$ are determined by solving

$$H_e\psi_i(\mathbf{r}_e;\mathbf{r}_p,\mathbf{R}) = \varepsilon_i(\mathbf{r}_p,\mathbf{R})\ \psi_i(\mathbf{r}_e;\mathbf{r}_p,\mathbf{R}) \tag{4}$$

Assuming N electronic states, we define $\vec{\psi}$ to be a column vector of the N electronic eigenfunctions $\{\psi_i(\mathbf{r}_e;\mathbf{r}_p,\mathbf{R})\}$ of eq 4. Then, we define an $N \times N$ transformation matrix $\mathbf{A}(\mathbf{r}_p;\mathbf{R})$ such that

$$\vec{\xi}(\mathbf{r}_e;\mathbf{r}_p,\mathbf{R}) = \mathbf{A}(\mathbf{r}_p;\mathbf{R})\ \vec{\psi}(\mathbf{r}_e;\mathbf{r}_p,\mathbf{R}) \tag{5}$$

where $\vec{\xi}$ is a column vector of functions satisfying the condition

$$\langle\xi_i|\nabla_{\mathbf{r}_p}\xi_j\rangle_e = 0 \text{ for all } i,j \tag{6}$$

Thus, the transformed electronic states $\{\xi_i(\mathbf{r}_e;\mathbf{r}_p,\mathbf{R})\}$ satisfy the standard definition of diabatic states with respect to the proton coordinate $\mathbf{r}_p$.

As discussed in refs 10 and 23, for a one-dimensional proton coordinate r_p and $N = 2$ electronic states, the matrix $\mathbf{A}$ is given by

$$\mathbf{A}(r_p;\mathbf{R}) = \begin{pmatrix} \cos\gamma & -\sin\gamma \\ \sin\gamma & \cos\gamma \end{pmatrix} \tag{7}$$

where

$$\gamma(r_p;\mathbf{R}) = \gamma(r_0;\mathbf{R}) - \int_{r_0}^{r_p} d_{12}^{(ep)}(r;\mathbf{R})\ dr \tag{8}$$

In this expression,

$$d_{12}^{(ep)}(r_p;\mathbf{R}) = \left\langle \psi_1 \middle| \frac{\partial\psi_2}{\partial r_p} \right\rangle_e = \frac{\left\langle \psi_1 \middle| \frac{\partial H_e}{\partial r_p} \middle| \psi_2 \right\rangle_e}{\varepsilon_2 - \varepsilon_1} \tag{9}$$

is the first-order nonadiabatic coupling between adiabatic electronic states 1 and 2, and $\gamma(r_0;\mathbf{R})$ is an additive constant that must be specified at some proton coordinate $r_p = r_0$. The diabatic potential energy matrix is given by $\mathbf{W} = \mathbf{AUA}^{-1}$, where $U_{ij} = \varepsilon_i(r_p,\mathbf{R})\delta_{ij}$

is the adiabatic potential energy matrix. Here, $W_{11}(r_p,\mathbf{R})$ and $W_{22}(r_p,\mathbf{R})$ are the diabatic electronic energies and $W_{12}(r_p,\mathbf{R})$ is the diabatic electronic coupling.

Previously, we applied this approach to symmetric systems. In this case, we chose $r_0 = 0$, corresponding to the transition state geometry, and set $\gamma(r_0) = -\pi/4$. This choice ensures that the adiabatic electronic states mix maximally and the diabatic electronic states cross at the transition state geometry, where the nonadiabatic coupling is a maximum. Moreover, the magnitude of the diabatic electronic coupling, W_{12}, is exactly half the splitting between the adiabatic electronic energies at this geometry. In the present paper, we extend this treatment to asymmetric systems, for which the nonadiabatic coupling is not necessarily a maximum at the transition state geometry. For the general case, we choose r_0 to be the hydrogen position at which the nonadiabatic coupling is maximum and set $\gamma(r_0) = -\pi/4$. This choice ensures that the diabatic states cross at $r_p = r_0$ and that the adiabatic states mix maximally at the hydrogen position corresponding to the largest nonadiabatic coupling.

II.B. Diabatization along Other One-Dimensional Reaction Coordinates. This approach may be extended to other one-dimensional reaction coordinates, such as a normal mode coordinate or an IRC. In this subsection, we discuss the generation of the diabatic electronic states along these types of alternative one-dimensional reaction coordinates, which typically are comprised of combinations of the motions of the transferring hydrogen and other heavy nuclei in the system. The objective is to calculate diabatic electronic states for which the first-order nonadiabatic coupling vanishes exactly along a general one-dimensional reaction coordinate. These diabatic electronic states will not be used to generate electron−proton vibronic states.

First, we discuss the generation of diabatic electronic states along a single normal mode coordinate, q, with corresponding effective mass μ. In this case, we can still utilize eqs 1−4 by replacing r_p with q and m_p with μ, where the adiabatic and diabatic electronic energies depend explicitly on q rather than r_p. In PCET reactions, the relevant normal mode describing the proton transfer reaction is expected to be dominated by proton motion, so typically $\mu \approx m_p$. The adiabatic-to-diabatic transformation given in eq 5 ensures that the component of the nonadiabatic coupling vector along the normal mode coordinate q vanishes. Since the normal mode coordinate is a linear combination of Cartesian displacements of all nuclei, the nonadiabatic coupling with respect to the normal mode coordinate can be calculated analytically as a linear combination of the nonadiabatic couplings with respect to the Cartesian coordinates of all nuclei.

An alternative one-dimensional reaction coordinate is the IRC, which is generated numerically by following the minimum energy path from a transition state to the corresponding reactant and product state minima. In this case, the theoretical formalism described above is no longer rigorous, but we are able to define the adiabatic-to-diabatic transformation given in eq 5 so that the component of the first-order nonadiabatic coupling vector along the IRC vanishes. Since the IRC is generally not a linear combination of Cartesian coordinates, the nonadiabatic coupling in eq 9 cannot be calculated analytically. Instead, the component of the nonadiabatic coupling vector along the IRC can be calculated numerically as the scalar product of the nonadiabatic coupling vector with respect to the Cartesian coordinates of all nuclei and the instantaneous displacement vector of these coordinates with respect to the IRC approximated at each point using central-point differentiation. The formal treatment of the IRC in terms of eqs 1−4 is not rigorously valid because the IRC is not associated with a specific mass and is not defined to have vanishing kinetic energy couplings with respect to other nuclear coordinates. As shown below, however, physically reasonable charge-localized diabatic electronic states for which the first-order nonadiabatic coupling vanishes along the IRC can be generated with this approach. Similarly, this approach may be used to generate these types of diabatic electronic states along any specified one-dimensional coordinate, such as the reaction path generated by a series of constrained optimizations, where the relative hydrogen position is constrained while all other nuclear coordinates are optimized.

II.C. Construction of Electron−Proton Vibronic States. The diabatic electronic energies and couplings may be used to construct the electron−proton vibronic states that form the basis of nonadiabatic PCET theories. In the case of one-dimensional hydrogen motion with fixed heavy nuclei $\mathbf{R}$, the proton vibrational states for diabatic electronic state i are obtained by solving

$$\left(-\frac{\hbar^2}{2m_p}\frac{\partial^2}{\partial r_p^2} + W_{ii}(r_p,\mathbf{R})\right)\varphi_\mu^{(i)}(r_p;\mathbf{R}) = \tilde{\varepsilon}_\mu^{(i)}(\mathbf{R})\,\varphi_\mu^{(i)}(r_p;\mathbf{R}) \tag{10}$$

where $\tilde{\varepsilon}_\mu^{(i)}(\mathbf{R})$ is the energy of the electron−proton vibronic state (i,μ). The diabatic electron−proton vibronic states $\{\zeta_{i\mu}(\mathbf{r}_e,r_p;\mathbf{R})\}$ are then defined as products of the diabatic electronic wave functions and associated proton vibrational wave functions:

$$\zeta_{i\mu}(\mathbf{r}_e,r_p;\mathbf{R}) = \xi_i(\mathbf{r}_e;r_p,\mathbf{R})\,\varphi_\mu^{(i)}(r_p;\mathbf{R}) \tag{11}$$

In the electronically nonadiabatic limit, the vibronic coupling between the reactant and product diabatic vibronic states $\zeta_{1\mu}$ and $\zeta_{2\nu}$ is[23,33,37]

$$V_{\mu\nu}^{(na)} = \langle\varphi_\mu^{(1)}|W_{12}|\varphi_\nu^{(2)}\rangle_p \tag{12}$$

which reduces to the familiar form of the diabatic electronic coupling multiplied by the Franck−Condon overlap between the reactant and product proton vibrational wave functions when the diabatic electronic coupling $W_{12}(r_p,\mathbf{R})$ is independent of r_p. In principle, a similar procedure could be applied to the diabatic electronic states generated along a normal mode coordinate when this normal mode is dominated by the hydrogen motion.

This treatment can be extended to construct three-dimensional electron−proton vibronic states that include the three-dimensional motion of the transferring hydrogen. In this case, the adiabatic and diabatic electronic states depend on the three-dimensional proton coordinate $\mathbf{r}_p = (r_p,s_p,t_p)$. The diabatic electronic states are constructed so that the component of the first-order nonadiabatic coupling vector along r_p, as given in eq 9, vanishes exactly for all points on a three-dimensional proton coordinate grid. Thus, the adiabatic-to-diabatic transformation can be expressed as

$$\vec{\xi}(\mathbf{r}_e;r_p,s_p,t_p,\mathbf{R}) = \mathbf{A}(r_p,s_p,t_p;\mathbf{R})\,\vec{\psi}(\mathbf{r}_e;r_p,s_p,t_p,\mathbf{R}) \tag{13}$$

but only the component of the first-order nonadiabatic coupling vector along r_p is used to determine $\mathbf{A}(r_p,s_p,t_p;\mathbf{R})$. In practice, the component of the first-order nonadiabatic coupling vector along r_p is calculated at each grid point (r_p,s_p,t_p). For each value of (s_p,t_p), r_0 is chosen to be the proton position along the r_p slice at which this nonadiabatic coupling is maximum, and $\gamma(r_p,s_p,t_p)$ is determined by calculating the line integral in eq 8 with $\gamma(r_0,s_p,t_p) = -\pi/4$. This procedure ensures that the first-order

nonadiabatic couplings with respect to r_p vanish exactly for all points on the three-dimensional proton coordinate grid.

The resulting three-dimensional diabatic potential energy matrix is given by $\mathbf{W} = \mathbf{AUA}^{-1}$, where $U_{ii} = \varepsilon_i(r_p,s_p,t_p,\mathbf{R})$ are the three-dimensional adiabatic potential energy surfaces and $W_{ii}(r_p,s_p,t_p,\mathbf{R})$ are the three-dimensional diabatic potential energy surfaces. For fixed heavy nuclei $\mathbf{R}$, the three-dimensional proton vibrational wave functions for diabatic electronic state i are calculated using the three-dimensional analog of eq 10 with potential energies $W_{ii}(r_p,s_p,t_p,\mathbf{R})$. These wave functions can then be combined with the associated diabatic electronic states, as in eq 11, to form three-dimensional electron−proton vibronic states.

We also explored an alternative more approximate formulation in which the adiabatic-to-diabatic transformation matrix $\mathbf{A}$ defined in eq 7 depends explicitly on only the one-dimensional proton coordinate r_p [i.e., $\gamma(r_p)$ is independent of the orthogonal coordinates (s_p,t_p)]. The advantage of this alternative formulation is that it only requires the calculation of the first-order nonadiabatic couplings along the one-dimensional r_p axis corresponding to $s_p = t_p = 0$ (i.e., the proton donor−acceptor axis in the applications discussed below). As a result, however, the first-order nonadiabatic couplings with respect to r_p vanish only along the one-dimensional r_p axis and do not vanish exactly for the other points on the three-dimensional proton coordinate grid.

II.D. Generalized Mulliken−Hush and Boys Localization. The GMH method[13,14] generates diabatic electronic states using the adiabatic electronic state dipole moments. These dipole moments are defined in terms of the adiabatic electronic states as $\vec{\mu}_{ij} = \langle\psi_i|\hat{\mu}|\psi_j\rangle$ for $i \in \{1,2\}$, where $\hat{\mu}$ is the dipole moment operator. The GMH method utilizes an adiabatic-to-diabatic transformation matrix analogous to eq 7:

$$\mathbf{A}^{\mathrm{GMH}}(r_p;\mathbf{R}) = \begin{pmatrix} \cos\theta & -\sin\theta \\ \sin\theta & \cos\theta \end{pmatrix} \tag{14}$$

In this case, $\theta(r_p;\mathbf{R})$ depends on the adiabatic electronic state dipole moments:

$$\tan(2\theta) = \frac{2\vec{\mu}_{12}\cdot\vec{v}}{|\vec{v}|^2} \tag{15}$$

where $\vec{v} = \vec{\mu}_{11} - \vec{\mu}_{22}$ and typically $\vec{\mu}_{12}$ and $\vec{v}$ are assumed to be parallel. Analogous to eq 5, the diabatic electronic states are determined by

$$\vec{\xi}^{\mathrm{GMH}}(\mathbf{r}_e;r_p,\mathbf{R}) = \mathbf{A}^{\mathrm{GMH}}(r_p;\mathbf{R})\,\vec{\psi}(\mathbf{r}_e;r_p,\mathbf{R}) \tag{16}$$

The GMH expression for the mixing angle in eq 15 is derived by defining $\mathbf{A}^{\mathrm{GMH}}$ as the transformation that diagonalizes the adiabatic dipole moment matrix, ensuring that the diabatic transition dipole moment is exactly zero, i.e., $\langle\xi_1^{\mathrm{GMH}}|\hat{\mu}|\xi_2^{\mathrm{GMH}}\rangle = 0$.

Subotnik et al. demonstrated that the GMH procedure can be extended to arbitrary geometries and multiple charge centers using Boys localization.[26] The more general expression for θ in eq 14 is given as[26]

$$\cos(4\theta) = \frac{-F}{\sqrt{F^2+G^2}} \tag{17}$$

where

$$F = |\vec{\mu}_{12}|^2 - \frac{|\vec{\mu}_{11}-\vec{\mu}_{22}|^2}{4} \tag{18}$$

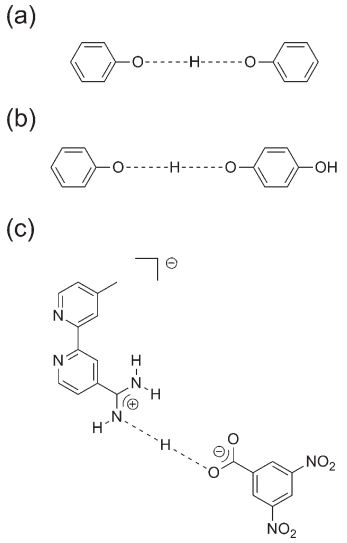

Figure 1. Three model systems studied: (a) phenoxyl−phenol, (b) phenoxyl−quinol, and (c) amidinium−carboxylate systems. The phenoxyl−phenol and phenoxyl−quinol systems are neutral, while the amidinium−carboxylate system has an overall charge of −1.

and

$$G = \vec{\mu}_{12}\cdot(\vec{\mu}_{11}-\vec{\mu}_{22}) \tag{19}$$

Invoking the assumption that $\vec{\mu}_{12}$ and $\vec{v}$ are parallel in eqs 17−19 leads to an expression for θ that coincides with the GMH expression given in eq 15.

III. COMPUTATIONAL METHODS

We used three systems to test the theoretical methods developed above. We studied the self-exchange reaction between the phenoxyl radical and the phenol molecule depicted in Figure 1a. We also studied the analogous reaction between the phenoxyl radical and the 1,4-benzenediol (quinol) molecule depicted in Figure 1b. The transition state geometries for these systems were calculated using density functional theory (DFT) with the B3LYP functional[38,39] and the 6-31G* basis set.[40] We also examined the amidinium−carboxylate system depicted in Figure 1c. We followed a similar but not identical geometry optimization procedure as that described in ref 36. In our procedure, we optimized the complete neutral amidinium−carboxylate system at the RHF/6-31G** level of theory, maintaining planarity of the system except for the three methyl group hydrogen atoms. The adiabatic and diabatic electronic states were calculated for the PCET reaction in the negatively charged complex with the lower proton in Figure 1c being transferred. The geometry optimizations were performed using Gaussian 09.[41]

We generated the adiabatic and diabatic electronic energy curves for the phenoxyl−phenol and phenoxyl−quinol systems along three different types of one-dimensional reaction coordinates. In the first scheme,[23] all nuclei except the transferring hydrogen atom were fixed at the transition state geometry, and the hydrogen was displaced along a one-dimensional grid spanning the hydrogen donor−acceptor axis. In the second scheme, all nuclei were displaced according to the normal mode coordinate corresponding to the negative frequency identified at the transition state geometry. In the third scheme, all nuclei were displaced according to the IRC calculated using the same level of

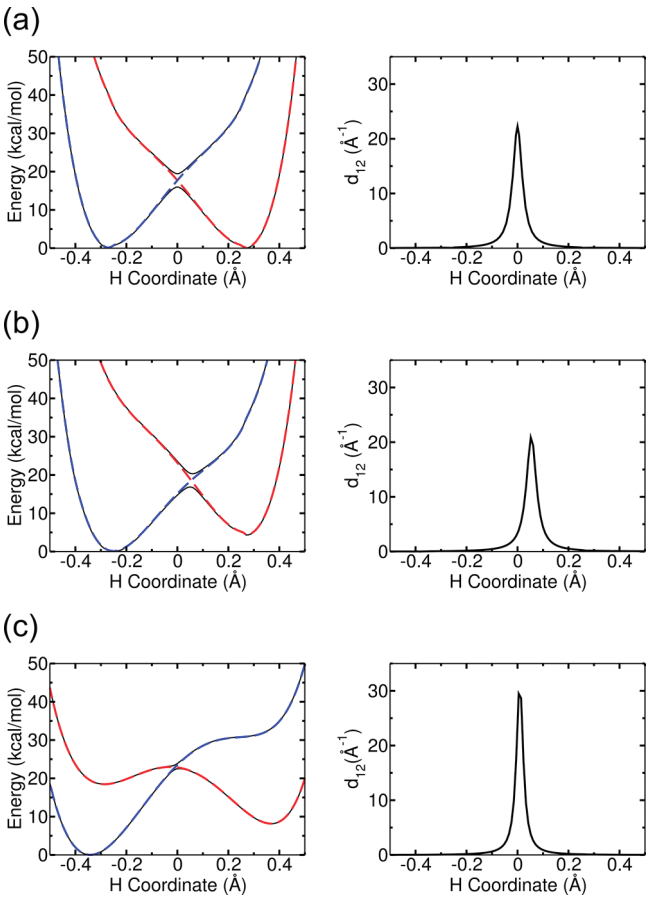

Figure 2. Adiabatic and diabatic electronic state properties as functions of the transferring hydrogen coordinate for the (a) phenoxyl−phenol, (b) phenoxyl−quinol, and (c) amidinium−carboxylate systems. The left panels depict the electronically adiabatic and diabatic potential energy curves. The solid black curves are the ground and first excited adiabatic state energies $\varepsilon_1(r_p,\mathbf{R})$ and $\varepsilon_2(r_p,\mathbf{R})$, respectively, calculated with the CASSCF method, and the dashed blue and red curves are the diabatic electronic energies $W_{11}(r_p,\mathbf{R})$ and $W_{22}(r_p,\mathbf{R})$, respectively, where the choice of $\gamma(r_0)$ is described in the text. The right panels depict the component of the first-order nonadiabatic coupling vector along the hydrogen donor−acceptor axis, as defined in eq 9.

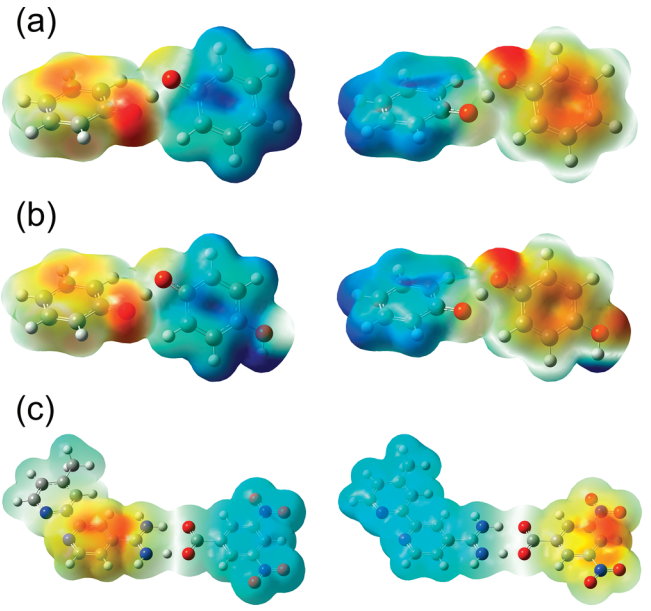

Figure 3. Electrostatic potential maps for the diabatic electronic states ξ_1 (left) and ξ_2 (right) corresponding to a density isosurface value of 0.005 for the (a) phenoxyl−phenol, (b) phenoxyl−quinol, and (c) amidinium−carboxylate systems at $r_p = r_0$. Negatively and positively charged regions are indicated by red and blue coloring, respectively. The maps for the amidinium−carboxylate system are difference electrostatic potential maps with respect to the neutral complex, as described in the text.

theory as described above. For all three schemes, we generated 128 geometries along the reaction coordinate. We used only the first scheme, which is based on the one-dimensional hydrogen coordinate along the hydrogen donor−acceptor axis with all other nuclei fixed, to study the amidinium−carboxylate system.

For each system, we calculated the two lowest-energy electronically adiabatic potential energy curves using the complete active space self-consistent field (CASSCF) method. The CASSCF calculations of the phenoxyl−phenol and phenoxyl−quinol systems were performed with the 6-31G* basis set and an active space of three electrons in six orbitals, state-averaging over the ground and first excited electronic states with equal weighting. The CASSCF calculations of the amidinium−carboxylate system were performed with the 6-31G** basis set and an active space of one electron in three orbitals, state-averaging over the lowest three electronic states with equal weighting.[36] We also calculated the two lowest-energy electronically adiabatic potential energy surfaces in three dimensions by displacing the hydrogen on a three-dimensional grid consisting of 16 points in each direction, with all other nuclei remaining fixed. In addition, we obtained the nonadiabatic coupling vectors with respect to the Cartesian coordinates of all nuclei directly from the CASSCF calculations. The GAMESS electronic structure package[42] was used to perform all CASSCF calculations. Note that these calculations were performed at a relatively low level of theory because our goal is to examine only the qualitative features of the various theoretical approaches.

We constructed the electron−proton vibronic states for one-dimensional or three-dimensional hydrogen motion with all other nuclei fixed. This procedure utilized the diabatic electronic states generated with the first scheme described above. We calculated one-dimensional proton vibrational wave functions describing the proton motion on the diabatic electronic energy surfaces by solving the one-dimensional Schrödinger equation given in eq 10. These calculations were performed with the Fourier grid Hamiltonian (FGH) method[43] using 128 grid points along the hydrogen donor−acceptor axis. We calculated three-dimensional proton vibrational wave functions using the three-dimensional analog of eq 10. These calculations were performed with the FGH−FCI (full configuration interaction) method[44] on the three-dimensional diabatic electronic energy surfaces mentioned above.

To examine the charge transfer properties, we calculated the dipole moments, atomic charges, and electrostatic potential maps as functions of the one-dimensional reaction coordinate for the adiabatic and diabatic electronic states. The properties of the adiabatic electronic states were calculated directly from the CASSCF wave functions with GAMESS. For the diabatic electronic states, we modified a local version of GAMESS to calculate these properties for the appropriate linear combination of configuration interaction states following the transformation

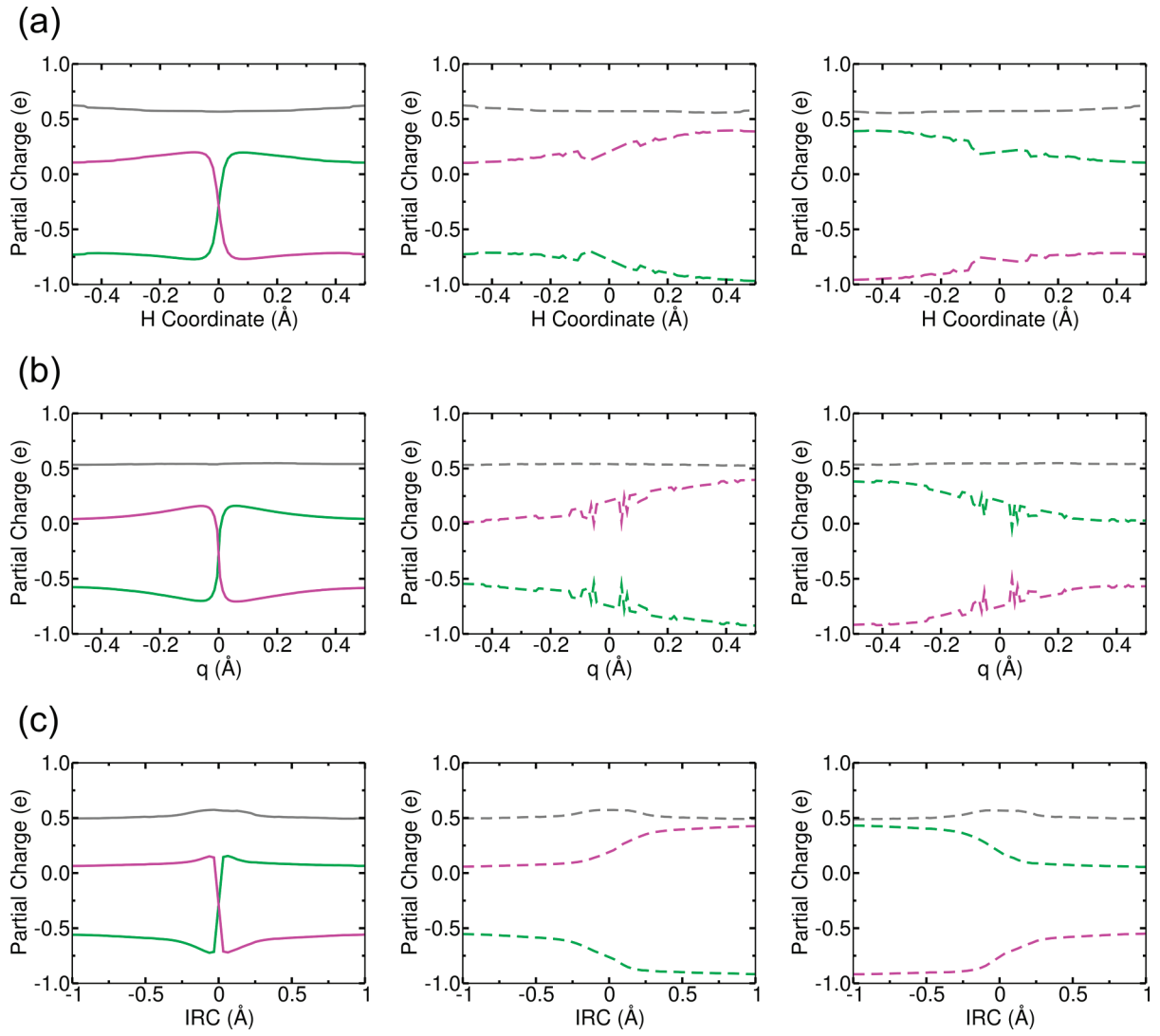

Figure 4. Partial charges determined from electrostatic potential-derived atomic charges for the ground adiabatic electronic state (left), the diabatic electronic state ξ_1 (center), and the diabatic electronic state ξ_2 (right) for the phenoxyl−phenol system calculated using various reaction coordinates: (a) the one-dimensional hydrogen coordinate, (b) the normal mode coordinate corresponding to the negative frequency at the transition state geometry, and (c) the IRC. Partial charges are shown for the donor molecule (green), acceptor molecule (purple), and transferring hydrogen (gray). Calculated values of the partial charges for the diabatic electronic states around $r_p = r_0$ are omitted due to numerical noise in this region.

given in eq 5. The atomic charges were obtained by fitting to the electrostatic potential calculated at points on the Connolly surface[45] under the constraint of reproducing the total charge and dipole moment of the electronic state under consideration.[46]

IV. RESULTS

IV.A. Generating Diabatic Electronic States. In this study, we applied the adiabatic-to-diabatic transformation methodology[23] to the more general case of asymmetric PCET reactions, as depicted in Figures 1b and c. For each system, we calculated the ground and first excited adiabatic electronic states and the nonadiabatic couplings along the one-dimensional hydrogen coordinate using the CASSCF method. As shown in Figures 2 and 3, the adiabatic-to-diabatic transformation successfully generated physically meaningful charge-localized diabatic electronic states for all three systems. In all cases, the diabatic electronic energies, $W_{11}(r_p,\mathbf{R})$ and $W_{22}(r_p,\mathbf{R})$ (dashed blue and red lines, respectively, in the left panels of Figure 2) are virtually identical to the adiabatic electronic energies, $\varepsilon_1(r_p,\mathbf{R})$ and $\varepsilon_2(r_p,\mathbf{R})$ (solid black lines in the left panels of Figure 2), over all hydrogen positions except near $r_p = r_0$, where they smoothly cross. All three systems exhibit a relatively localized region of strong nonadiabatic coupling, as shown in the right panels of Figure 2.

Figures 2b and c illustrate that the phenoxyl−quinol and the amidinium−carboxylate systems possess significantly asymmetric adiabatic electronic energies and nonadiabatic couplings. In particular, these systems exhibit an energy bias between geometries corresponding to the hydrogen localized on the donor molecule and the hydrogen localized on the acceptor molecule. Furthermore, the maximum of the nonadiabatic coupling along the donor−acceptor axis is shifted from the donor−acceptor midpoint, which is chosen to be at $r_p = 0$ for all systems. This shift is more noticeable for the phenoxyl−quinol system. As mentioned above, we chose r_0 to be the hydrogen position at which the nonadiabatic coupling is maximum and set

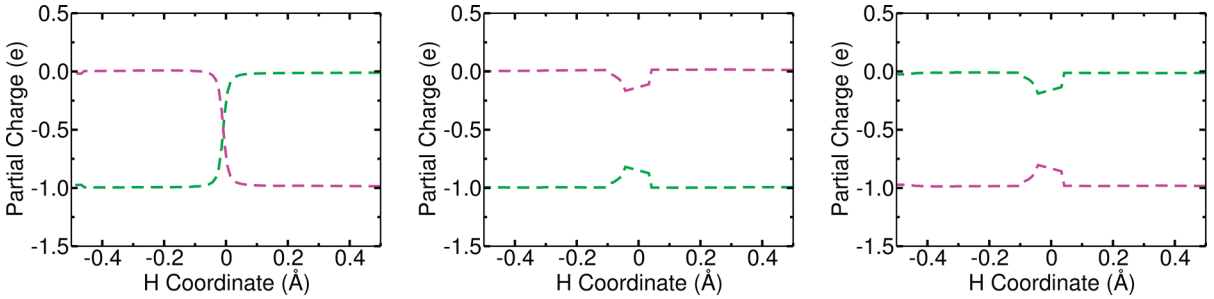

Figure 5. Partial charges determined from electrostatic potential-derived atomic charges for the ground adiabatic electronic state (left), the diabatic electronic state ξ_1 (center), and the diabatic electronic state ξ_2 (right) as functions of the transferring hydrogen coordinate for the amidinium−carboxylate system. Partial charges are shown for the donor molecule (green) and the acceptor molecule (purple). The partial charges on the donor and acceptor molecules are obtained after subtracting the corresponding partial charges of the neutral complex, as described in the text. Due to this subtraction, the transferring hydrogen has no significant charge, although it has a nearly constant charge of ∼0.58*e* for the adiabatic and diabatic electronic states prior to this subtraction. Calculated values of the partial charges for the diabatic electronic states around $r_p = r_0$ are omitted due to numerical noise in this region.

$\gamma(r_0) = -\pi/4$ in eq 8 to ensure that the diabatic states cross at $r_p = r_0$ and that the adiabatic states mix maximally at the hydrogen position corresponding to the largest nonadiabatic coupling. Figure 2 illustrates that the resulting diabatic potential energies correspond to the transferring hydrogen localized on the donor molecule in $W_{11}(r_p,\mathbf{R})$ and the acceptor molecule in $W_{22}(r_p,\mathbf{R})$.

The electrostatic potential maps for diabatic states ξ_1 and ξ_2 at $r_p = r_0$ are depicted in Figure 3. These electrostatic potential maps illustrate that the diabatic electronic states possess localized electronic charge distributions. The corresponding electrostatic potential maps for other positions of the transferring hydrogen are provided in the Supporting Information (Figures S1−S3) and indicate that these electronic charge distributions are relatively invariant along the transferring hydrogen coordinate. The amidinium−carboxylate system is negatively charged, and the electrostatic potential maps are strongly influenced by the charge separation at the hydrogen-bonding interface (see Figure 1c). To clarify the charge localization of the diabatic electronic states with respect to the transferring electron, the electrostatic potential of the neutral amidinium−carboxylate complex was subtracted from that of the negatively charged complex. The resulting difference electrostatic potential maps plotted in Figure 3 clearly demonstrate charge localization with respect to the transferring electron.

Figures 4a and 5 depict the partial charges on the donor (green) and acceptor (purple) molecules for the adiabatic (left panels) and diabatic (center and right panels) electronic states for the phenoxyl−phenol and amidinium−carboxylate systems, respectively. The corresponding figure for the phenoxyl−quinol system is provided in Supporting Information Figure S4. For all three systems, the partial charges on the donor and acceptor molecules change significantly along the reaction coordinate for the adiabatic electronic states but remain relatively constant for the diabatic electronic states. Analogous to the procedure used for the electrostatic potential maps, the partial charges for the donor and acceptor molecules in the amidinium−carboxylate system are determined by subtracting the corresponding partial charges calculated for the neutral complex. The partial charges prior to this subtraction are provided in Supporting Information Figure S5. As shown in Figure 5, the resulting plots clearly demonstrate the charge localization of the diabatic electronic states with respect to the transferring electron. Thus, this adiabatic-to-diabatic transformation method provides physically

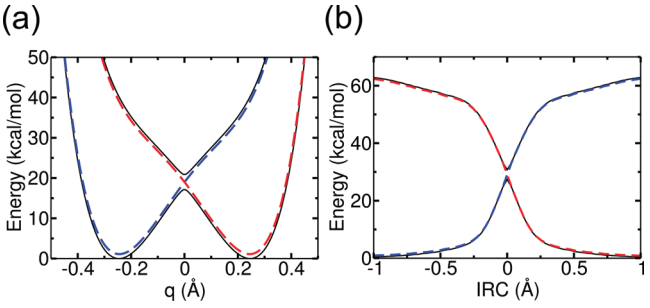

Figure 6. Electronically adiabatic and diabatic potential energy curves for the phenoxyl−phenol system as functions of (a) the normal mode coordinate corresponding to the negative frequency at the transition state geometry and (b) the IRC. The solid black curves are the ground and first excited adiabatic state energies, and the dashed blue and red curves are the diabatic electronic energies.

meaningful diabatic electronic states with localized electronic charge distributions that are relatively invariant along the transferring hydrogen coordinate for both symmetric and asymmetric systems.

We also calculated the diabatic electronic states along two other types of reaction coordinates: the normal mode coordinate associated with the negative frequency at the transition state and the IRC. We present the results for the phenoxyl−phenol system, although the corresponding results for the asymmetric phenoxyl−quinol system are qualitatively similar to those for the symmetric case and are included in Supporting Information Figure S6. Figure 6 depicts the adiabatic and diabatic electronic energies calculated along the normal mode coordinate and the IRC. We observed that the normal mode coordinate is dominated by the motion of the transferring hydrogen (i.e., the mass associated with this normal mode was ∼1.12 amu). For this reason, the adiabatic and diabatic electronic energies calculated along the normal mode coordinate (Figure 6a) are very similar to those calculated along the one-dimensional hydrogen coordinate (Figure 2a). The adiabatic and diabatic electronic energies calculated along the IRC (Figure 6b) are qualitatively similar to those calculated along the one-dimensional hydrogen coordinate near the transition state but plateau in the outer regions after the IRC reaches the minimum energy geometries.

Figure 4 compares the partial charges on the donor (green) and acceptor (purple) molecules for the adiabatic (left panels)

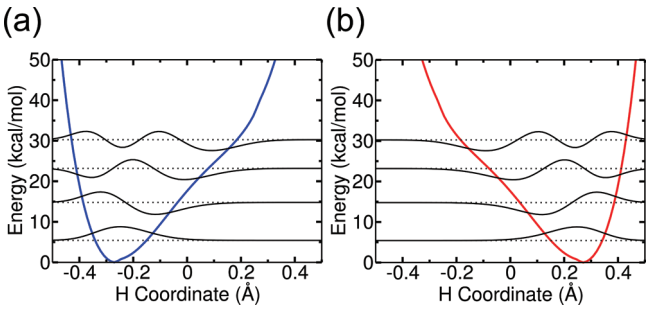

Figure 7. Four lowest-energy one-dimensional proton vibrational wave functions (black solid lines) calculated using eq 10 for the diabatic electronic potential (a) W_{11} and (b) W_{22} for the phenoxyl−phenol system.

and diabatic (center and right panels) electronic states for the three different types of reaction coordinates. The partial charges for the one-dimensional hydrogen coordinate and the normal mode coordinate, as depicted in Figures 4a and b, respectively, are very similar. The results for the IRC are also qualitatively similar. In all cases, the partial charges on the donor and acceptor molecules remain relatively constant along the reaction coordinate for the diabatic electronic states. Thus, the adiabatic-to-diabatic transformation method provides charge-localized diabatic electronic states with electronic charge distributions that are relatively invariant along all three types of reaction coordinates.

IV.B. Constructing Electron−Proton Vibronic States. We constructed the electron−proton vibronic states corresponding to the diabatic electronic states generated along the one-dimensional hydrogen coordinate with all other nuclei fixed. For this purpose, we calculated the one-dimensional proton vibrational wave functions by solving eq 10 with each of the diabatic electronic energies, $W_{11}(r_p,\mathbf{R})$ and $W_{22}(r_p,\mathbf{R})$, shown in Figure 2a. The four lowest-energy proton vibrational wave functions corresponding to each diabatic electronic state for the phenoxyl−phenol system are depicted in Figure 7. These proton vibrational wave functions can be combined with the diabatic electronic wave functions, ξ_1 and ξ_2, by forming products as in eq 11 to obtain the electron−proton vibronic states that comprise the basis of nonadiabatic PCET rate theories. In particular, these vibronic states can be used directly to calculate vibronic couplings, which are essential for the calculation of experimentally accessible quantities such as rate constants and kinetic isotope effects. The vibronic couplings calculated using eq 12 will be discussed below.

We also calculated three-dimensional diabatic potential energy surfaces and the associated proton vibrational wave functions. For this purpose, we applied the adiabatic-to-diabatic transformation given by eq 13, where the transformation matrix depends on the three-dimensional proton coordinate, and the component of the nonadiabatic coupling vector along r_p vanishes exactly for all points on the three-dimensional proton coordinate grid. The resulting partial charges for the phenoxyl−phenol system are given in Table 1. For comparison, we also applied the more approximate adiabatic-to-diabatic transformation, where the transformation matrix depends explicitly on only the one-dimensional proton coordinate r_p, and the component of the nonadiabatic coupling vector along r_p vanishes exactly only for points on the one-dimensional proton donor−acceptor axis. The resulting partial charges are given in Table S1 of the Supporting Information and are qualitatively similar to those provided in Table 1. This more approximate approach may be useful for larger systems because the computational expense is significantly lower.

Table 1. Average Electrostatic Potential-Derived Partial Charges Calculated for the Three-Dimensional Ground Adiabatic and Diabatic Electronic States Reported with Standard Deviations for the Phenoxyl−Phenol System[a]

electronic state	donor charge	acceptor charge	H charge
ψ_1	-0.2 ± 0.4	-0.2 ± 0.4	0.5 ± 0.1
ξ_1	-0.7 ± 0.2	0.3 ± 0.2	0.4 ± 0.1
ξ_2	0.3 ± 0.2	-0.7 ± 0.2	0.4 ± 0.1

[a] The tabulated results were computed by averaging over the 16^3 hydrogen positions on the three-dimensional grid, where points around $r_p = r_0$ were omitted due to numerical noise in this region. All charges are given in units of e. Deviation of the total charge from zero is due to numerical noise and round-off error. The diabatic electronic states were calculated using eq 13, ensuring that the component of the first-order nonadiabatic coupling vector along r_p vanishes exactly for all points on the three-dimensional grid.

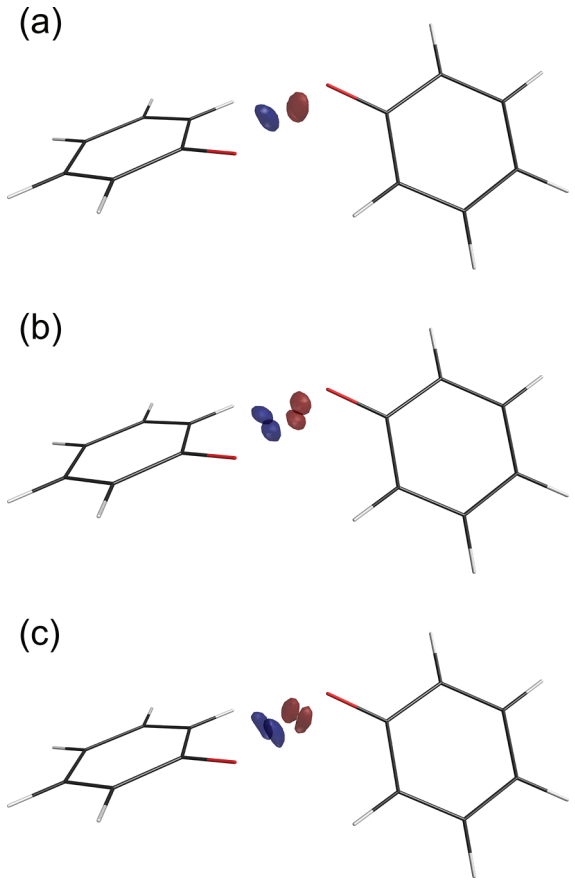

Figure 8. Three lowest-energy three-dimensional proton vibrational wave functions corresponding to a density isosurface value of 0.002 for the three-dimensional diabatic potential energy surfaces W_{11} (blue wave functions) and W_{22} (red wave functions) for the phenoxyl−phenol system. The top figure corresponds to the lowest-energy proton vibrational state.

Table 1 demonstrates that the three-dimensional diabatic electronic states generated for the phenoxyl−phenol system

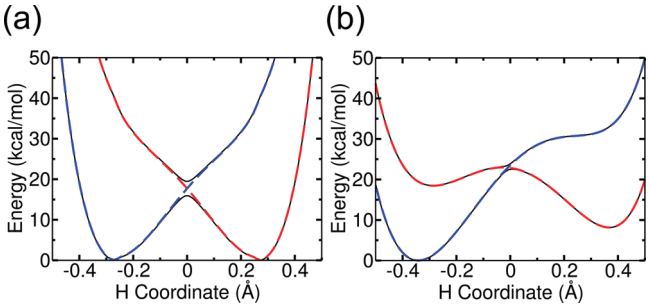

Figure 9. Electronically adiabatic and diabatic potential energy curves for (a) the phenoxyl−phenol system and (b) the amidinium−carboxylate system as functions of the hydrogen coordinate calculated using the GMH method. The solid black curves are the ground and first excited adiabatic state energies, and the dashed blue and red curves are the diabatic electronic energies.

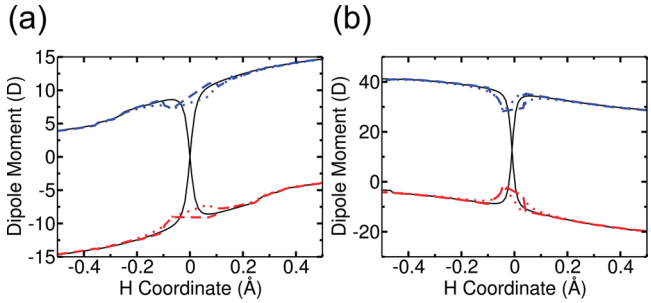

Figure 10. Component of the dipole moment vector along the hydrogen donor−acceptor axis for the ground and first excited adiabatic electronic states (solid black curves) and the diabatic electronic states ξ_1 (blue) and ξ_2 (red) for the (a) phenoxyl−phenol system and (b) amidinium−carboxylate system calculated using the GMH method (dotted) and the adiabatic-to-diabatic transformation method described in section II.A (dashed). A positive (negative) dipole moment indicates a dipole moment vector pointing toward the acceptor (donor). The origin was chosen to be $r_p = 0$ for the amidinium−carboxylate system.

are charge-localized. This table provides the partial charges on the donor and acceptor molecules, as well as the transferring hydrogen, averaged over all hydrogen positions on the three-dimensional grid. As expected, the average donor and acceptor partial charges for the three-dimensional adiabatic electronic ground state are identical, and the standard deviations reflect the changes in the donor and acceptor partial charges that are consistent with those observed along the one-dimensional hydrogen coordinate depicted in the left panel of Figure 4a. In contrast, the three-dimensional diabatic electronic states exhibit charge-localization: the average charge on the donor is negative (positive) and the average charge on the acceptor is positive (negative) when averaged over all hydrogen positions for the diabatic electronic state ξ_1 (ξ_2). These results are also consistent with the partial charges along the one-dimensional hydrogen coordinate depicted in the center and right panels of Figure 4a. The standard deviations are slightly larger than would be predicted from Figure 4 because of numerical fluctuations near the transition state geometry.

We used these three-dimensional diabatic potential energy surfaces to calculate the associated three-dimensional proton vibrational wave functions with the FGH−FCI method. The three lowest-energy proton vibrational wave functions corresponding to each diabatic electronic state for the phenoxyl−phenol system are depicted in Figure 8. The proton vibrational wave functions associated with the diabatic state ξ_1 (blue) are localized near the donor molecule, while the proton vibrational wave functions associated with the diabatic state ξ_2 (red) are localized near the acceptor molecule. These results are consistent with the corresponding one-dimensional proton vibrational wave functions along the donor−acceptor axis depicted in Figure 7. The three-dimensional proton vibrational wave functions can be combined with the corresponding diabatic electronic wave functions to generate three-dimensional diabatic electron−proton vibronic states, which can be used to calculate vibronic couplings, rate constants, and kinetic isotope effects of nonadiabatic PCET reactions.

IV.C. Comparison to Generalized Mulliken−Hush and Boys Localization. We also used the GMH procedure to generate charge-localized diabatic electronic states for the phenoxyl−phenol and amidinium−carboxylate systems. The adiabatic state dipole moments were calculated directly from the CASSCF wave functions. The GMH diabatization produced qualitatively similar diabatic electronic states to those generated using the diabatization procedure described in section II.A. In particular, the diabatic electronic energies depicted in Figures 9a and b are virtually identical to those depicted in Figures 2a and c, respectively. Moreover, Figure 10 illustrates that the calculated diabatic state dipole moments are very similar for the two diabatization schemes. Thus, these two fundamentally different diabatization approaches lead to nearly identical diabatic electronic states. In principle, proton vibrational wave functions could be calculated using the GMH diabatic potential energies and combined with the associated diabatic electronic wave functions to form electron−proton vibronic states, as described above.

In addition, we used the Boys localization scheme to generate diabatic electronic states for the phenoxyl−phenol and amidinium−carboxylate systems. The Boys localization method produced results that are virtually identical to the GMH results presented in Figures 9 and 10. This high level of agreement is attributed to the observation that the vectors $\vec{\mu}_{12}$ and $\vec{\mu}_{11} - \vec{\mu}_{22}$ were essentially parallel for all positions of the transferring hydrogen. In particular, for all r_p such that $|r_p| \leq 0.5$ Å, $|(\vec{\mu}_{12})^u \cdot (\vec{\mu}_{11} - \vec{\mu}_{22})^u| \geq 0.998$ for the phenoxyl−phenol system and $|(\vec{\mu}_{12})^u \cdot (\vec{\mu}_{11} - \vec{\mu}_{22})^u| \geq 0.992$ for the amidinium−carboxylate system, where the u superscript indicates the unit vector in the specified direction. Thus, the GMH and Boys localization methods are in excellent agreement with the diabatization method presented in section II.A for the systems studied.

Finally, we calculated the electronic coupling at the geometry corresponding to the crossing point of the diabatic potential energy curves for the three systems studied. This quantity, $W_{12}(r_0;\mathbf{R})$, is calculated as the off-diagonal element of the diabatic potential energy matrix obtained from transforming the adiabatic potential energy matrix at $r_p = r_0$. Table 2 demonstrates that the electronic couplings calculated using the GMH and Boys localization methods agree very well with those obtained from the diabatization procedure described in section II.A. Table 2 also provides the vibronic couplings between the ground electron−proton vibronic states calculated using eq 12 for $\mu = \nu = 0$. These vibronic couplings are significantly smaller than the corresponding electronic couplings because of the relatively small overlap

Table 2. Electronic and Vibronic Couplings Calculated at the Geometry Corresponding to the Crossing Point of the Diabatic Potential Energy Curves Using the Various Diabatization Methods[a]

system	V_{el}^{GMH}	V_{el}^{Boys}	V_{el}	$V_{00}^{(na)}$
phenol	606	606	606	7.2
quinol	610	610	611	8.7
amidinium−carboxylate	205	205	206	0.44

[a] The electronic couplings were calculated as the off-diagonal element of the diabatic potential energy matrix at $r_p = r_0$ using the GMH method, the Boys localization method, and the method described in Section IIA for V_{el}^{GMH}, V_{el}^{Boys}, and V_{el}, respectively. The vibronic couplings $V_{00}^{(na)}$ between ground electron−proton vibronic states were calculated with V_{el} using eq 12 for $\mu = \nu = 0$. All couplings are given in units of cm^{-1}.

between the reactant and product ground state proton vibrational wave functions.

V. CONCLUSIONS

In this paper, we developed a scheme to generate charge-localized diabatic electronic states for a wide range of PCET systems. These charge-localized diabatic electronic states are obtained from standard electronic structure calculations using an adiabatic-to-diabatic transformation designed to ensure that the first-order nonadiabatic couplings with respect to a specified one-dimensional reaction coordinate vanish exactly. We applied this protocol to both symmetric and asymmetric PCET systems with several different one-dimensional reaction coordinates, including the hydrogen transfer coordinate, a normal mode coordinate, and the IRC. This approach was also extended to construct three-dimensional charge-localized diabatic electronic surfaces corresponding to the three-dimensional motion of the transferring hydrogen. We demonstrated that this methodology leads to physically meaningful charge-localized diabatic electronic states with relatively invariant charge distributions along the reaction coordinate. These diabatic electronic states are in excellent agreement with those obtained from the GMH and Boys localization methods.

In addition, we combined these diabatic electronic states with the associated proton vibrational wave functions to generate electron−proton vibronic states that describe one- or three-dimensional hydrogen motion. These electron−proton vibronic states can be used to calculate the vibronic couplings that enter the nonadiabatic rate constant expressions for PCET reactions. Within the golden rule formalism, each term in the nonadiabatic PCET rate constant expression is proportional to the square of the electron−proton vibronic coupling for a pair of reactant and product vibronic states. As a result, the vibronic couplings strongly impact the rate constants and kinetic isotope effects of PCET reactions. Thus, the construction of charge-localized electron−proton vibronic states is essential for the calculation of experimentally measurable quantities such as the rate constants and kinetic isotope effects of PCET reactions.

■ ASSOCIATED CONTENT

Supporting Information. Electrostatic potential maps corresponding to the diabatic electronic states at different positions of the transferring hydrogen for all three systems studied; partial charges of the donor molecule, acceptor molecule, and transferring hydrogen for the adiabatic and diabatic electronic states of the phenoxyl−quinol system and of the amidinium−carboxylate system prior to subtraction of the corresponding charges for the neutral system; adiabatic and diabatic electronic state energies along a normal mode coordinate and the IRC for the phenoxyl−quinol system; average partial charges of the donor molecule, acceptor molecule, and transferring hydrogen for the three-dimensional adiabatic and diabatic electronic states of the phenoxyl−phenol system using the alternative more approximate approach; coordinates of the phenoxyl−quinol and amidinium−carboxylate systems. This material is available free of charge via the Internet at http://pubs.acs.org.

■ AUTHOR INFORMATION

Corresponding Author
*E-mail: shs@chem.psu.edu.

■ ACKNOWLEDGMENT

We thank Alexander Soudackov and Anirban Hazra for helpful discussions and advice. We gratefully acknowledge funding from NSF grants CHE-07-49646 and CHE-10- 57875. A.S. thanks the Natural Sciences and Engineering Research Council of Canada for a PGS scholarship.

■ REFERENCES

(1) Cukier, R. I.; Nocera, D. G. *Annu. Rev. Phys. Chem.* **1998**, *49*, 337–369.
(2) Hammes-Schiffer, S.; Soudackov, A. V. *J. Phys. Chem. B* **2008**, *112*, 14108–14123.
(3) Hammes-Schiffer, S.; Stuchebrukhov, A. A. *Chem. Rev.* **2010**, *110*, 6939–6960.
(4) Huynh, M. H. V.; Meyer, T. J. *Chem. Rev.* **2007**, *107*, 5004–5064.
(5) Mayer, J. M. *Annu. Rev. Phys. Chem.* **2004**, *55*, 363–390.
(6) Hammes-Schiffer, S. *Acc. Chem. Res.* **2001**, *34*, 273–281.
(7) Soudackov, A.; Hammes-Schiffer, S. *J. Chem. Phys.* **2000**, *113*, 2385–2396.
(8) Soudackov, A.; Hatcher, E.; Hammes-Schiffer, S. *J. Chem. Phys.* **2005**, *122*, 014505.
(9) Atchity, G. J.; Ruedenberg, K. *Theor. Chem. Acc.* **1997**, *97*, 47–58.
(10) Baer, M. *Chem. Phys. Lett.* **1975**, *35*, 112–118.
(11) Baer, M. *Mol. Phys.* **1980**, *40*, 1011–1013.
(12) Baer, M. *Phys. Rep.-Rev. Sec. Phys. Lett.* **2002**, *358*, 75–142.
(13) Cave, R. J.; Newton, M. D. *Chem. Phys. Lett.* **1996**, *249*, 15–19.
(14) Cave, R. J.; Newton, M. D. *J. Chem. Phys.* **1997**, *106*, 9213–9226.
(15) Cembran, A.; Song, L. C.; Mo, Y. R.; Gao, J. L. *J. Chem. Theory Comput.* **2009**, *5*, 2702–2716.
(16) Nakamura, H.; Truhlar, D. G. *J. Chem. Phys.* **2001**, *115*, 10353–10372.
(17) Nakamura, H.; Truhlar, D. G. *J. Chem. Phys.* **2002**, *117*, 5576–5593.
(18) Newton, M. D. *Chem. Rev.* **1991**, *91*, 767–792.
(19) Pacher, T.; Cederbaum, L. S.; Koppel, H. *J. Chem. Phys.* **1988**, *89*, 7367–7381.
(20) Pacher, T.; Cederbaum, L. S.; Koppel, H. *Adv. Chem. Phys.* **1993**, *84*, 293.
(21) Papas, B. N.; Schuurman, M. S.; Yarkony, D. R. *J. Chem. Phys.* **2008**, *129*, 124104.
(22) Ruedenberg, K.; Atchity, G. J. *J. Chem. Phys.* **1993**, *99*, 3799–3803.
(23) Sirjoosingh, A.; Hammes-Schiffer, S. *J. Phys. Chem. A* **2011**, *115*, 2367–2377.
(24) Song, L. C.; Mo, Y. R.; Gao, J. L. *J. Chem. Theory Comput.* **2009**, *5*, 174–185.

(25) Subotnik, J. E.; Cave, R. J.; Steele, R. P.; Shenvi, N. *J. Chem. Phys.* **2009**, *130*, 234102.
(26) Subotnik, J. E.; Yeganeh, S.; Cave, R. J.; Ratner, M. A. *J. Chem. Phys.* **2008**, *129*, 244101.
(27) Thiel, A.; Koppel, H. *J. Chem. Phys.* **1999**, *110*, 9371–9383.
(28) Van Voorhis, T.; Kowalczyk, T.; Kaduk, B.; Wang, L. P.; Cheng, C. L.; Wu, Q. *Annu. Rev. Phys. Chem.* **2010**, *61*, 149–170.
(29) Wu, Q.; Van Voorhis, T. *J. Chem. Phys.* **2006**, *125*, 164105.
(30) Wu, Q.; Van Voorhis, T. *J. Chem. Theory Comput.* **2006**, *2*, 765–774.
(31) Zhu, X. L.; Yarkony, D. R. *J. Chem. Phys.* **2010**, *132*, 104101.
(32) Hammes-Schiffer, S. *ChemPhysChem* **2002**, *3*, 33–42.
(33) Skone, J. H.; Soudackov, A. V.; Hammes-Schiffer, S. *J. Am. Chem. Soc.* **2006**, *128*, 16655–16663.
(34) Kirby, J. P.; Roberts, J. A.; Nocera, D. G. *J. Am. Chem. Soc.* **1997**, *119*, 9230–9236.
(35) Roberts, J. A.; Kirby, J. P.; Nocera, D. G. *J. Am. Chem. Soc.* **1995**, *117*, 8051–8052.
(36) Soudackov, A.; Hammes-Schiffer, S. *J. Am. Chem. Soc.* **1999**, *121*, 10598–10607.
(37) Georgievskii, Y.; Stuchebrukhov, A. A. *J. Chem. Phys.* **2000**, *113*, 10438–10450.
(38) Becke, A. D. *J. Chem. Phys.* **1993**, *98*, 5648–5652.
(39) Lee, C. T.; Yang, W. T.; Parr, R. G. *Phys. Rev. B* **1988**, *37*, 785–789.
(40) Hariharan, P. C.; Pople, J. A. *Theor. Chim. Acta* **1973**, *28*, 213–222.
(41) Frisch, M. J.; Trucks, G. W.; Schlegel, H. B.; Scuseria, G. E.; Robb, M. A.; Cheeseman, J. R.; Scalmani, G.; Barone, V.; Mennucci, B.; Petersson, G. A.; Nakatsuji, H.; Caricato, M.; Li, X.; Hratchian, H. P.; Izmaylov, A. F.; Bloino, J.; Zheng, G.; Sonnenberg, J. L.; Hada, M.; Ehara, M.; Toyota, K.; Fukuda, R.; Hasegawa, J.; Ishida, M.; Nakajima, T.; Honda, Y.; Kitao, O.; Nakai, H.; Vreven, T.; Montgomery, J. A.; Peralta, J. E.; Ogliaro, F.; Bearpark, M.; Heyd, J. J.; Brothers, E.; Kudin, K. N.; Staroverov, V. N.; Kobayashi, R.; Normand, J.; Raghavachari, K.; Rendell, A.; Burant, J. C.; Iyengar, S. S.; Tomasi, J.; Cossi, M.; Rega, N.; Millam, J. M.; Klene, M.; Knox, J. E.; Cross, J. B.; Bakken, V.; Adamo, C.; Jaramillo, J.; Gomperts, R.; Stratmann, R. E.; Yazyev, O.; Austin, A. J.; Cammi, R.; Pomelli, C.; Ochterski, J. W.; Martin, R. L.; Morokuma, K.; Zakrzewski, V. G.; Voth, G. A.; Salvador, P.; Dannenberg, J. J.; Dapprich, S.; Daniels, A. D.; Farkas; Foresman, J. B.; Ortiz, J. V.; Cioslowski, J.; Fox, D. J. *Gaussian 09*, Revision B.01; Gaussian Inc.: Wallingford, CT, 2009.
(42) Schmidt, M. W.; Baldridge, K. K.; Boatz, J. A.; Elbert, S. T.; Gordon, M. S.; Jensen, J. H.; Koseki, S.; Matsunaga, N.; Nguyen, K. A.; Su, S. J.; Windus, T. L.; Dupuis, M.; Montgomery, J. A. *J. Comput. Chem.* **1993**, *14*, 1347–1363.
(43) Marston, C. C.; Balint-Kurti, G. G. *J. Chem. Phys.* **1989**, *91*, 3571–3576.
(44) Webb, S. P.; Hammes-Schiffer, S. *J. Chem. Phys.* **2000**, *113*, 5214–5227.
(45) Connolly, M. L. *J. Appl. Crystallogr.* **1983**, *16*, 548–558.
(46) Singh, U. C.; Kollman, P. A. *J. Comput. Chem.* **1984**, *5*, 129–145.